MICHIGAN VERTICAL FLIGHT TECHNOLOGY

VFS DBVF 2020-2021 Final Technical Report

MICHIGAN ENGINEERING
UNIVERSITY OF MICHIGAN

ALTAIR

Ford

SIEMENS
Ingenuity for life

BLUE ORIGIN

Executive Summary

Michigan Vertical Flight Technology (MVFT) is a student project team from the University of Michigan competing in the 2020-2021 Vertical Flight Society (VFS) Design-Build-Vertical Flight (DBVF) Competition. The team consists of 26 members that range from first-year undergraduate students to graduate students pursuing a Master's degree. The objective of the team is to produce an aircraft that successfully meets all requirements presented by the competition Request for Proposal (RFP), providing students with hands-on experience in electric vertical take-off and landing (eVTOL) aircraft development.

The purpose of this aircraft design is to provide a platform that can take off vertically, transition between vertical and cruise flight quickly, and sustain cruise flight over large distances efficiently. The aircraft must have a maximum take-off weight (MTOW) under 9 kg (20 lbs), carry a payload of at least 0.9 kg (2 lbs), have a maximum dimension under 2 m (6.6 ft), use a commercial off-the-shelf (COTS) lithium polymer (LiPo) battery of 6 cells (6S) or less, provide a manual shunt plug for power cut-off that is at least 6 inches away from the rotors, and demonstrate a kill switch with lost-link power cut functionality.

To demonstrate the success of these requirements without an in-person fly-off component of competition, MVFT will conduct flight tests at the Flying Pilgrims RC Model Club that simulate the Maneuverability, Maximum Range, and Autonomy Bonus Challenge courses presented by the competition.

To begin the project cycle, MVFT conducted initial trade studies throughout September and early October 2020 that compared design options that fit the objectives, purpose, and requirements of the aircraft described above. Two key trade studies included an analysis of the performance of various rotor layouts, and a wing configuration study to determine the airframe form factor that is most efficient for cruise flight performance. These trade studies led to a tilt-rotor tricopter rotor configuration with a blended wing body (BWB) for fast and efficient cruise flight. The results of the trade studies also identified various technical innovations that the team has incorporated, including servo-controlled tilt-mechanisms for vectored thrust, autonomous capabilities for landing accuracy, and an autopilot-assisted cruise stability control using differential thrust.

Once the trade studies were completed, the team moved into initial design of the competition aircraft and prototype selection. A tilt-rotor configuration was desirable for its efficiency between VTOL and fixed-wing flight by using the same propulsion system for both flight stages, but this had not been attempted by MVFT in the past. MVFT decided to construct a sub-scale prototype, "NM-1", of the competition aircraft to begin flight testing in November 2020 to quickly verify the choice of this configuration. This also provided a platform to test a variety of tilt-rotor mechanisms, leading to the decision to use a direct-drive tilt-rotor servo located directly inside the motor pivot.

Through a Systems Engineering Leadership course that the team is involved in, MVFT conducted a Preliminary Design Review (PDR) on October 22, 2020 to receive feedback from the team's advisors and a panel of industry experts. This provided valuable insight into the design, and confirmed the team's ability to proceed with detailed design of the aircraft at the component level. Additionally, the Power and Propulsion sub-teams completed the design and began the construction of a custom thrust test stand that has allowed the team to extensively test various combinations of propulsion and power components that would identify the most efficient power and propulsion systems that meet the aircraft requirements.

After detailed design was complete, a Critical Design Review (CDR) was conducted on February 2, 2021 in the same fashion as PDR, which approved the team's suggestion to move forward with aircraft construction, thrust testing, and continued prototype testing. In addition, the team used a custom quadcopter fashioned with the same autopilot as the sub-scale prototype and competition aircraft to conduct autonomy testing on a low-risk platform. This testing has been successful, and provided valuable information for improving the procedure and accuracy of autonomous waypoint navigation.

At the time of this report, the team has completed all ground testing for aircraft component selection, successfully demonstrated vertical flight maneuvers on the sub-scale prototype, successfully demonstrated autonomous waypoint navigation from take-off to landing on the quadcopter, manufactured the competition aircraft, and bench tested the competition aircraft to confirm readiness for final flight testing.

A Flight Readiness Review (FRR) will be held in a similar fashion to PDR and CDR on March 31, 2021, to further refine the team's progress and plans for the final flight testing program. Between the time of this report's submission and the final presentation on April 16, 2021, MVFT will conduct autonomy testing with the sub-scale prototype, complete transition and cruise flight testing with the sub-scale prototype, and complete all flight testing necessary to demonstrate the required competition aircraft performance capabilities mentioned in this executive summary.

1. Management Summary

The management of MVFT during the 2020-2021 academic year is broken into technical sub-teams and officer positions, as seen in Figure 1 on page 3 below. The technical sub-teams include Airframe, Avionics, Operations, Power, and Propulsion.

Due to the complexity and workload, the Airframe sub-team is divided into Aerodynamics and Structures, but remains one sub-team due to the continuous collaboration required between the two groups. Aerodynamics conducts studies on the initial aerodynamic sizing of the aircraft, design of the surface features, analysis of the aerodynamic performance, and study of the craft's stability. Structures is responsible for the structural design and FEA of the internal frame, which includes integration at the component level and interfacing between major subsystems to ensure proper connections, weights, and balances. MVFT's Avionics sub-team is focused on the control system development of the aircraft, which includes the construction and flight testing of sub-scale prototypes to verify the aircraft configuration, manual control, and autonomous functionality.

The Power sub-team is responsible for the design and implementation of power system development to meet the capacity and discharge requirements of each electrical component, including the wire routing and connections. Propulsion is responsible for the design and testing of the propulsion configuration, with a large focus on thrust testing with Power to determine the best combination of electronic speed controllers (ESCs), motors, and propellers to meet aircraft requirements. The Operations sub-team plays both a systems engineering and administrative role, with responsibilities that include communication between sub-teams for subsystem integration, tracking of major timelines with respect to sub-system development, and management of team sponsors.

Figure 1. MVFT 2020-2021 management organization chart

The President is the lead officer, who has responsibilities that include guidance of high-level team goals and activities, purchasing of materials, and organization of the budget. A Risk Manager tracks the risk of the team using a living document for the Failure Mode and Effects Analysis (FMEA) at the component level. Finally, the Social Media Director manages the team image and online presence, ensuring that sponsorship recognition is complete. MVFT receives direct advising from its technical advisor, Dr. Carlos Cesnik, and its operations advisor, Professor George Halow, along with help from an industry panel of experts at PDR, CDR, and FRR. A project cycle trade study can be seen in Figure 2 below.

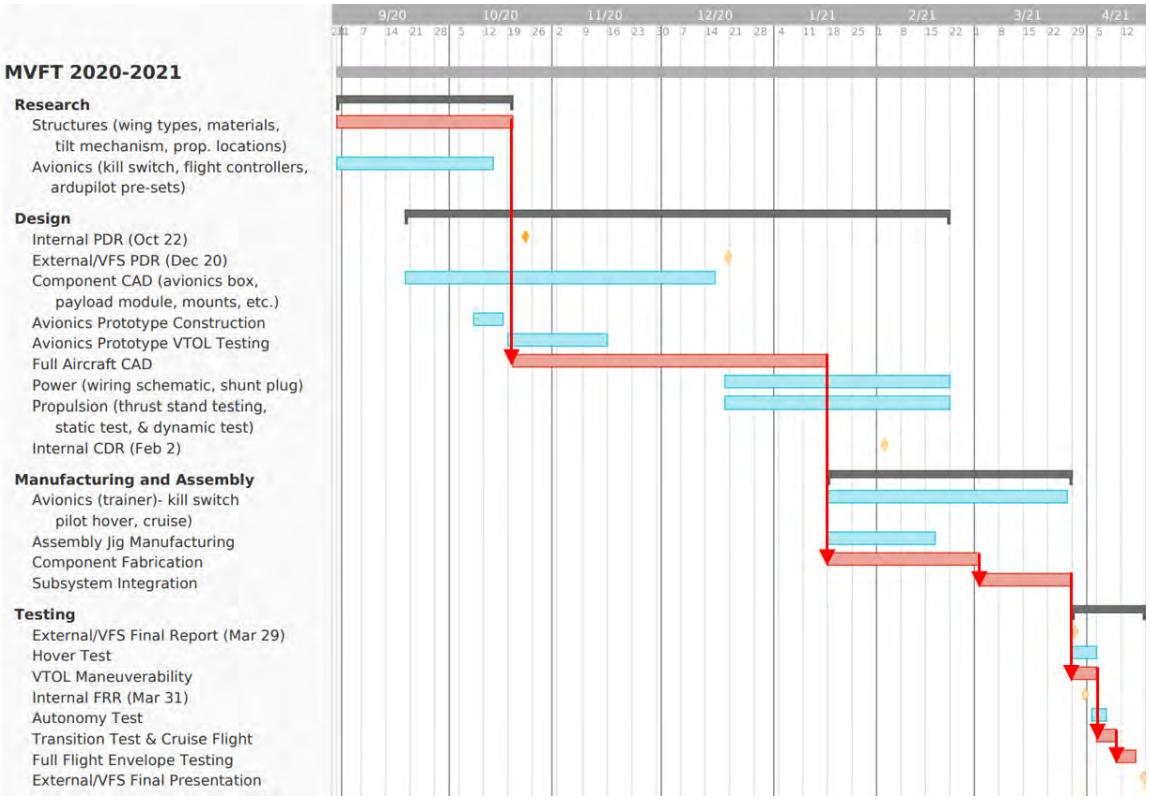

Figure 2. MVFT team Gantt chart for the 2020-2021 project cycle

2. Design Trade Studies

2.1 Initial Aircraft Configuration Decision Matrix

To refine the trade studies for more detailed research, an initial decision matrix that can be seen in below was created by the team. After identifying the potential designs that the team could pursue, parameters were created to quantify the usability of the design. Each of these parameters were given a weight depending on how important the parameter was for success in competition and success for the team's goals, and the results of the tool can be seen below in Table 1.

Design / Parameter	Tricopter Three Tilt-Rotor	Tricopter Two Tilt-Rotor	Quadcopter Tail-Sitter	Bicopter Elevon Tail-Sitter	Bicopter Tilt-Rotor Tail-Sitter	Quad Two-Phase
Size	18	22	12	32	32	4
Weight	24	26	28	36	32	12
Hover Efficiency	61.75	66.5	47.5	76	76	33.25
Cruise Efficiency	24	24	20	24	24	20
Avionics Availability	25	24	25	25	25	25
Maneuverability	21	18	12	9	18	15
Manufacturability	30.25	33	55	44	35.75	38.5
Complexity	48.75	48.75	56.25	67.5	48.75	52.5
Hover Stability	60	52	64	16	16	64
Transition Ability	71.25	66.5	28.5	9.5	19	80.75
Payload Fraction	12	13	14	8	8	4
UAM Safety	7.5	8.25	4.5	1.5	1.5	10.5
UAM Passenger Experience	5	5	1	1	1	8
Score:	408.5	407	367.75	349.5	337	367.5

Table 1. Initial decision matrix for ranking potential aircraft configurations for further study

2.2 Rotor Layout

To assist in aircraft decision making, the team began trade studies by researching bicopter, tricopter, quadcopter, and Y6 (shown in Figure 3) configurations. MVFT gathered propeller data [1] on a variety of diameters to calculate the power draw for aircraft masses between 4.5 kg (10 lb) and 9 kg (20 lb). The propeller data was used to determine which configuration would balance power draw and system weight with the focus on hover since the power consumption in cruise should be significantly lower because only a small component of thrust goes towards lifting the aircraft [2].

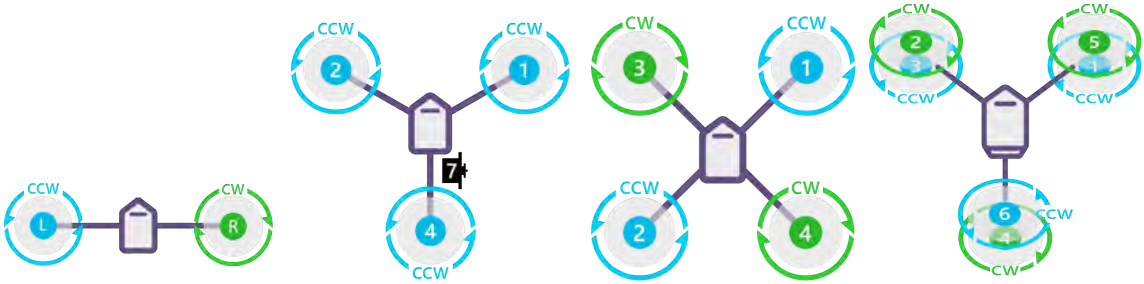

Figure 3. Aircraft rotor configurations. Left to right: Bicopter, Tricopter, Quadcopter, Y6. Colors represent rotation direction and numbers indicate channel mapping to flight controller [3]

From the collected data, MVFT determined which propeller option requires the least amount of power to sustain hover given an aircraft mass. Using the propeller options, the team found sample motors for each

option to estimate the total mass of the propulsion system. By combining the propulsion mass and the power draw, the team was able to qualitatively compare which configuration would result in the lowest mass of propulsion and power combined. In the future, this analysis should be improved to keep the disk loading of each configuration constant and compare more directly what the mass contribution from each configuration would be.

Based on Figure 4, the tricopter minimizes the power draw and propulsion system weight. The bicopter has small disc loading without drastically increasing the rotor diameter, so it requires much higher power as the aircraft weight increases [4]. During the trade studies, the disk loading was not kept constant, which, next year, will be a factor the team works to make uniform. The distinguishing factor is the mass of the system and the tricopter minimizes the weight as it has fewer components. Therefore, the tricopter with a 51-cm propeller was selected as the final propulsion system.

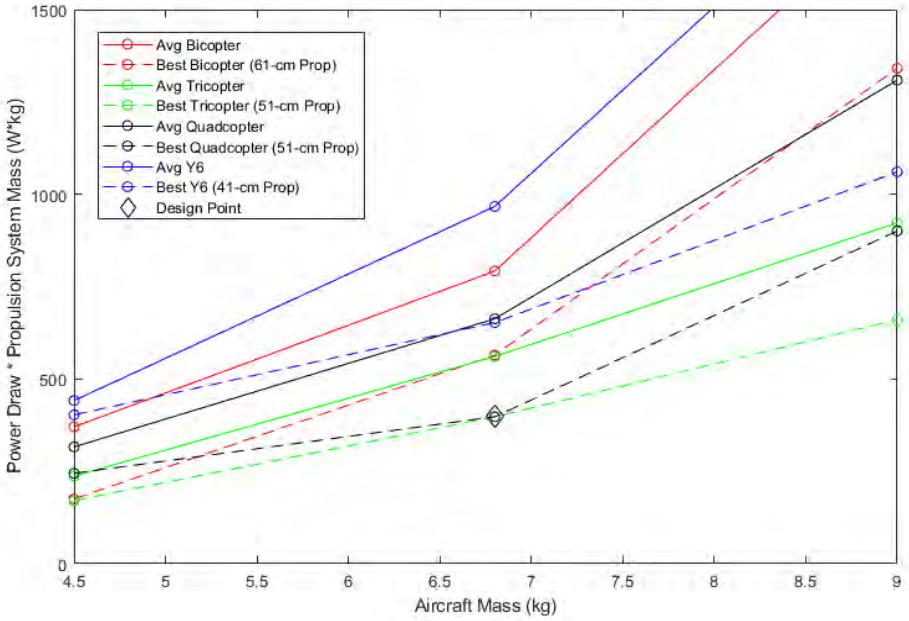

Figure 4. Best and average power draw × system mass of each configuration vs aircraft mass.

2.3 Wing Configuration Trade Study

The wings considered were a blended wing body (BWB), a tube and wing (TW), and a wingless design. Performance of winged and wingless designs were evaluated with respect to the different components of the competition: cruise, hover, and payload capacity. The team determined that the advantage of a winged design is that it increases flight time by 2x and range by 10x, and is therefore preferred over the increased hover efficiency and smaller payload projected area of a wingless design. [5], [6], [7], [8].

TW designs obtain their lift efficiency for having a high aspect ratio (AR) while BWB designs obtain their efficiency for the overall reduction in wetted area and form drag.[9] To ensure cruise lift efficiency, conventional aspect ratios (AR) were chosen for TW and BWB, which were 8 and 4 respectively. For these AR values and a desired 2g banked turn with a structural safety factor (SF) of 1.5, the TW and BWB designs are evaluated against the competition dimension requirement, as shown in Figure 5.

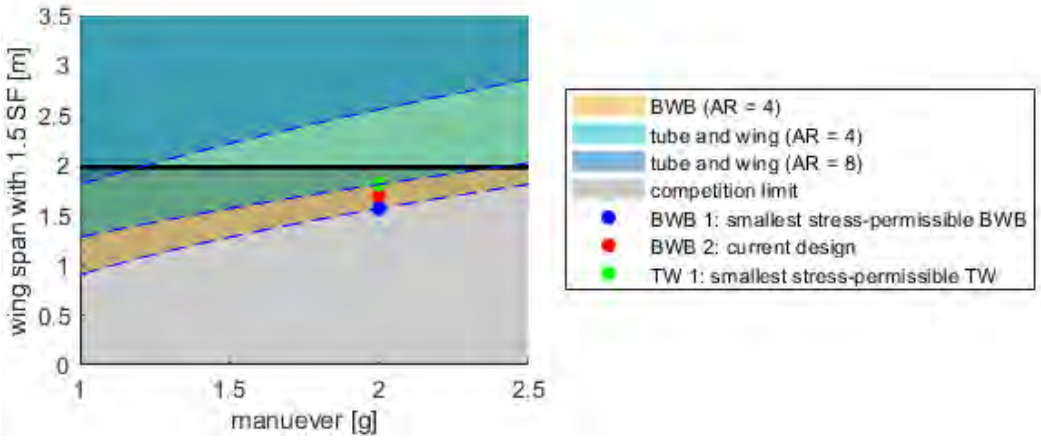

Figure 5. Wing span comparison of BWB and TW with the chosen AR values and a maximum desired stress of 287 N/m^2 based on prior experience for aircraft consisting of wood and composite materials.

For the chosen tricopter configuration presented in section 2.1, three designs (also indicated in Figure 5) were scaled to fit the chosen rotors and payloads while maintaining a 2g maneuver load and complying to the maximum dimension requirement (Table 2). The current design is larger than BWB 1 due to the need to fit all internal payloads. Their respective empennages are scaled by typical volume coefficients and the component weights were estimated using Raymer's method [9].

	Fuselage	Horizontal Tail	Vertical Tail	Wing	**Total Mass (kg)**	**Mass comparison**
BWB 1	-	-	0.02	0.45	**0.47**	**60%**
BWB 2	-	-	0.07	0.66	**0.73**	**93%**
TW 1	0.25	0.06	0.02	0.46	**0.79**	**100%**

Table 2. Estimated mass breakdown (kg) of BWB and TW designs.

In general, with a set stress constraint and incorporation of internal components, BWB would be lighter than TW. Additionally, the TW design analyzed here compromises the lift efficiency for its AR 4 wing. Thus, from the analyses, the BWB is the most desirable for its cruise efficiency and mass.

3. Technical Innovations

3.1 Servo-Controlled Tilt Mechanisms

Multiple iterations were tested to find the best method for integrating a tilt-rotor mechanism that was strong enough to handle the loads, remained lightweight, and minimized the wetted area below the propellers in vertical flight that would cause a reduction in thrust. After these iterations, MVFT will make use of direct-drive servo-controlled tilt mechanisms on all three motors of the aircraft. These allow the pilot to have full control of the aircraft in vertical flight with only 3 motors instead of the conventional 4 motors seen on quadcopters. Yaw input will be provided by tilting the front 2 motors in opposite directions, and this thrust vectoring provides significantly more yaw authority than MVFT has seen on previous aircraft built by the team. With a tilt-rotor transition method, the aircraft will use the same motors for vertical and horizontal flight, improving efficiency. This increases the weight margin of the aircraft, providing more weight allocation to the payload and power system.

Another advantage of tilting all three motors is that the maximum thrust can be used to accelerate the aircraft when transitioning from vertical to horizontal flight, providing a higher transition stage

acceleration. Since the motors must be capable of tilting in both directions for yaw authority, this tilt range can also be used to slow down the aircraft when transitioning from horizontal to vertical flight. These performance advantages are expected to drastically improve the aircraft performance in the Maximum Range and Maneuverability courses for competition. There was an interesting suggestion in the feedback that MVFT received after the VFS PDR submission, suggesting that the rear motor does not need to be tilted due to the reduced thrust requirements during horizontal flight. This would provide an efficiency advantage for horizontal flight, and will be tested by the team after this competition cycle. For this year, MVFT has chosen to proceed with all 3 motors tilting for the aforementioned acceleration benefits during transition.

3.2 Autopilot Landing Capabilities

A servo-controlled FPV system was considered to improve landing accuracy on approach during the Maneuverability Course, but controlling this would further complicate the job of the pilot. Instead, MVFT decided to keep a stationary forward-facing FPV camera and use an Ardupilot-compatible LiDAR sensor located on the bottom of the aircraft. This will measure vertical distance from the landing surface once the aircraft is within 8 meters of the landing point and show the altitude on the FPV screen for pilot reference. Active weathervaning is a valuable feature of Ardupilot that will be used during VTOL flight, which assists the autopilot with position accuracy by yawing the aircraft to turn the nose into the direction of the wind. This reduces the drag on the aircraft in hover, and allows for more accurate landings.

3.3 Differential Thrust for Cruise Maneuver Stability

Due to the tailless configuration and the lack of rudder, the team expected adverse yaw to be present in a banked turn, which was also later confirmed in the stability analysis presented in section 4.1.3. More specifically, due to the increased drag on the higher wing of the banked aircraft, the craft would yaw away from the turn. Thus, more directional authority is obtained from the use of differential thrust where the thrust on the higher wing would be increased to counteract the drag and maintain the yaw throughout the turn. This will be done using the FLY BY WIRE_A (FBWA) mode in Ardupilot that maintains the attitude of a turn by controlling the throttle of the propellers in place of a rudder for yaw control.

3.4 Cruise Speed and Propulsion Requirements

To optimize the cruise speed of the aircraft to maximize laps and payload fraction, the team simulated the power requirements and lap times for a range of cruise speeds between the stall speed and 44.7 m/s (100 mph). From the lift-drag curve (section 4.1.2), thrust necessary for the steady-level flight was determined, where the reference area is 0.7 m^2, air density is 1.22 kg/m^3 , and the mass of the aircraft is 7.71 kg. With the drag on the craft, propulsive power can be calculated by multiplying the thrust and airspeed together, to which a 60% efficiency factor was applied to determine the electrical power needed to supply the motor. Next, using an assumption for 30 seconds total for takeoff and landing per lap, the maximum number of laps fully completed in 10 minutes was calculated based on a constant cruise speed and the length of the course, shown in Figure 6. Similarly, the time in hover vs cruise for each cruise speed was used to calculate the total amount of energy required by the propulsion system. Using the specific energy of a Lipo of 150.5 W*h/kg, the necessary battery mass was calculated.

Once the battery mass and maximum lap count were determined for each cruise speed, the team investigated the battery mass at the minimum cruise speed to complete 12, 13, and 14 laps, resulting in a cruise speed of 24.5, 30.5, and 38 m/s respectively. The team also determined that each additional lap results in roughly 100 g extra battery mass required for the mission. Therefore, to balance the reduced payload capacity with increased number of laps, the team decided on a cruise speed of 30.5 m/s since the speed required for 14 laps would be too difficult to control on the small course. It is also worth reducing

the payload capacity by 100 g which corresponds to a 1.3% change in payload to increase the lap count by 8.3% by completing 13 laps instead of 12. At this cruise speed, the propulsion system must be capable of 550 g of thrust at 30.5 m/s, corresponding to roughly 150 W per motor.

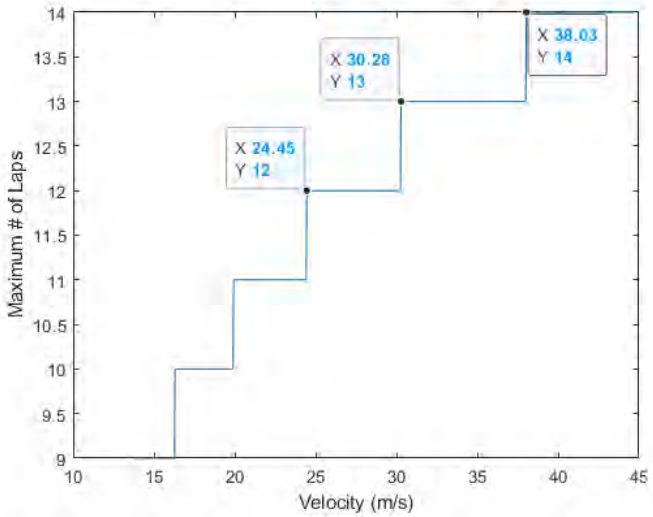

Figure 6. Plot of maximum number of laps possible at each cruise speed

3.5 Shunt Plug Mechanism

To save electrical losses, weight, and the need for the wings to carry large gauge wire, MVFT developed a mechanism allowing the electrical shunt plug to remain inside the fuselage while the accessible pull tab is located on the edge of the left wing, outside of the 6 inch propeller box outlined in the requirements. A custom mounting bracket and attachment system were designed that allows the shunt plug to be aligned with the hollow spar running to the edge of the left wing and easily disengaged should there be a need to quickly power down the system. This can be seen in Figure 16.

4. Design Definition

4.1 Airframe

4.1.1 Structures

The aircraft has a wingspan of 1699 *mm.* Its maximum outstretched dimension is from the rear tip of one winglet to the opposite front propeller sweep in the cruise flight configuration, and this dimension is 1960 *mm*. Therefore, in any configuration, the aircraft remains within the competition size requirement of 1981 *mm*. The airframe was built around a stiff carbon fiber frame, and the load paths exist along this internal frame. The frame is shown in Figure 7, along with the expected load paths.

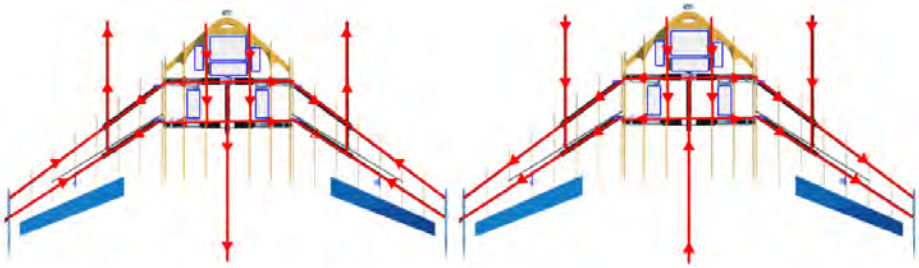

Figure 7. Aircraft structural load paths for vertical flight mode (left) and cruise flight mode (right). In the vertical configuration the weight of the craft is supported by the propellers, whereas in cruise mode the weight is distributed to the wings.

Maximal expected loads on the airframe for analysis were determined to be the following:

1. In the vertical configuration, a vertical acceleration of 2G produced by the propulsion system. This may be accompanied by a precession moment at the tilting mechanism from tilting the spinning propellers. Approximating the propeller as a uniform rod and assuming a spin rate of 6000 *RPM* and a tilt rate of 18 *RPM* (calculated based on characteristics of the selected tilt servo) gives a worst-case estimate of 1.6 *Nm* applied to the tilt mechanism perpendicular to the tilt axis from precession, and 1.6 *Nm* applied between the links of the tilting mechanism along the tilt axis (Figure 8).
2. In the cruise configuration, a bank turn in which aerodynamic forces produce 2G of acceleration vertically in the body-fixed frame (Figure 8).

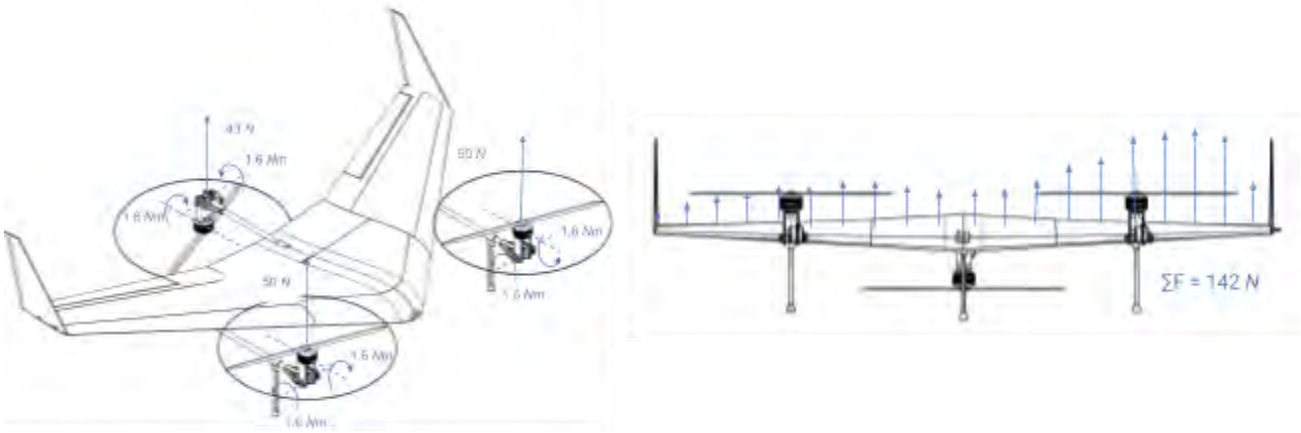

Figure 8. Visualization of maximal loads in cases 1 (left) and 2 (right).

To design for both cases, analyses were performed using the FEA software Altair Inspire on isolated regions of the structure. For Case 1, the frame and tilting mechanism were isolated in two separate models. To verify the frame, the expected vertical load and horizontal moments were applied to the ends of the propulsion booms, with a support placed at the aircraft CG. To verify the tilting mechanism, the same loads were applied at the propulsion motor attachment point with supports at the attachment point to the propulsion boom. For Case 2, the frame and ribs were isolated. Strip forces pulled from the aerodynamic model in AVL under the specified 2G maneuver were applied to the ribs, and a support was placed at the aircraft CG. In both models, all parts were shown to have at least a 1.5 safety factor on admissible loads. Additionally, For Case 1 angular deflection from propeller precession loads was shown to be less than 1°. This was acceptable as the aircraft control system should be able to compensate for errors in thrust vector direction caused by deflections of this magnitude.

The aircraft, loaded with the prescribed 0.90 kg (2 lb) of payload, was estimated using the Siemens NX built-in mass properties calculator, along with the estimated mass budgets of systems not reflected in the CAD model. The aircraft has a total takeoff mass of 7.6 kg, with the CG 290 mm aft of the nose.

4.1.2 Aerodynamics

The lift and drag characteristics were predicted using Athena Vortex Lattice (AVL) developed by MIT [10]. Lift and drag estimates predicted using AVL are shown in Figure 9.

The cruise velocity is relatively far away from the stall point, providing a sufficient range in angle of attack and velocity to achieve the various flight conditions, such as a 60° banked turn. Target cruise, turn, and stall conditions are listed in Table 3.

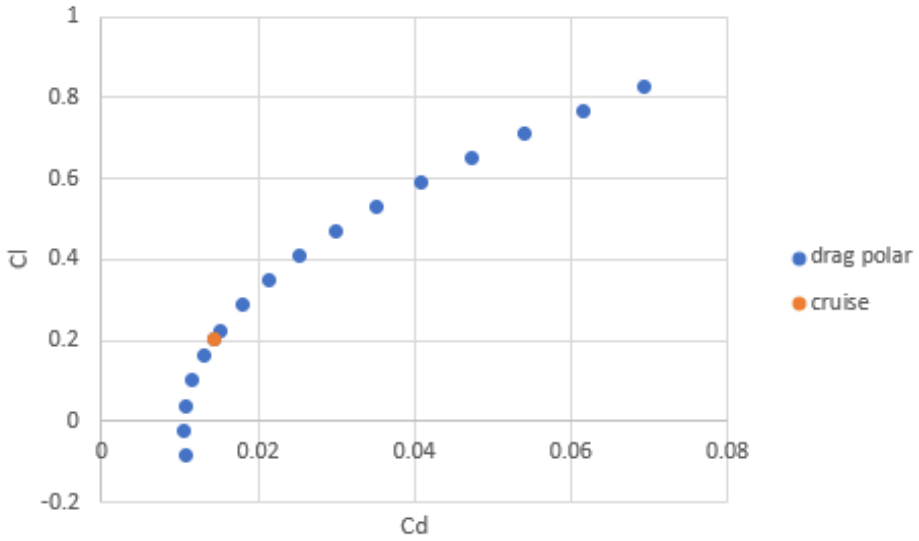

Figure 9. Drag polar of airframe configuration predicted by AVL.

	Cruise	60° Banked Turn	Stall
Angle of attack	2.7°	11.1°	13°
Velocity	30 m/s	22 m/s	14 m/s
C_L	0.2	0.76	0.83
C_D	0.014	0.065	0.069
Max sectional C_l	0.37	2.00	1.6
Elevon deflection	0°	10°	0°

Table 3. Lift and drag characteristics as estimated by AVL.

The stall condition is determined by the critical section method where stall is declared when any point of the wing reaches a local C_l of 1.6, which is the maximum lift coefficient of the chosen airfoils (MH78 and L188tip). Similarly, since the aircraft is fixed-winged, the turning radius is relatively large, approximately 30 m. The turning condition is then determined as the near-minimum speed where the elevons are not in stall. The maximum local lift coefficient for those sections is augmented by 0.7 due to the elevons, which are separated from the wing by a small spanwise gap. [11] Since AVL does not predict parasitic drag of the vehicle, an additional 0.01 $C_{D,\,parasitic}$ is taken into account when simulating the flight conditions.

AVL was advantageous for fast design iterations, however, at the expense of accuracy. Therefore, STAR CCM+ is used to verify the estimates at nominal cruise and stall determined by AVL. The angle of attack and drag estimates are compared at each condition in Table 4 for the same C_L.

	Nominal AVL Cruise		Nominal AVL Stall		Stall observed in STAR CCM+	
	STARCCM+	% diff compared to AVL	STARCCM+	% diff compared to AVL	STARCCM+	% diff compared to AVL
α	2.7°	-29%	14°	-15%	17°	-16%
C_L	0.26	0%	0.77	0%	0.91	0%
C_D	0.014	17%	0.030	69%	0.051	47%
C_L/C_D	19	10%	26	211%	18	44%

Table 4. Angle of attack and drag estimate comparison between AVL and STAR CCM+

In STAR CCM+ simulations, flow separation was not observed at the nominal AVL stall angle of 14° but at 17° instead. Overall, compared to STAR CCM+, AVL overestimates the drag and underestimates the angle, which would suggest that it could fly at a higher angle of attack than anticipated and would experience less drag. However, since the booms or landing gear were not modeled, a more conservative estimate is advantageous, in which the cruise propulsion requirements are based on the AVL predictions.

4.1.3 Stability

Static and dynamic stability are also examined using AVL. Longitudinally, the neutral point is estimated to be 0.42 m from the nose, which provides approximately 18% static margin. Laterally, the stability derivatives are $C_{l\beta} = -0.106 < 0$ and $C_{n\beta} = 0.0719 > 0$. These coefficients and parameters suggest that the vehicle is statically stable. Dynamically, the poles of the aircraft are plotted in Figure 10.

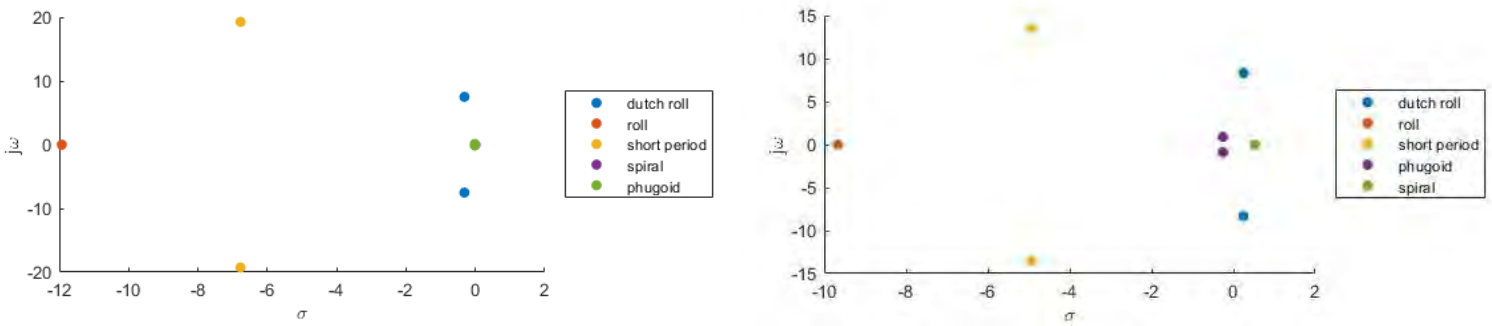

a. Dyn. stability modes in cruise b. Dyn. stability modes 60° banked turn

Figure 10.. Dynamic stability in cruise and at banked turn.

The vehicle is dynamically stable in all modes in cruise and in a 60° banked turn except for the spiral and dutch roll modes during the turn. As the dutch roll mode is also present in NM1 and was able to be tuned out using PID, the PID controller will be used to resolve the dutch roll instability. Regarding the spiral instability, differential thrust will be used to coordinate turning and maintain the yaw angle.

4.2 Propulsion

The propulsion system of the aircraft consists of three rotors mounted on a pivot, allowing transition between hover and conventional flight. To select the components for the propulsion system, a variety of motors, ESCs, and propellers were tested to determine the lightest and most efficient system. The configuration was required to produce at least a 2:1 Thrust-to-Weight ratio (TWR) to ensure the aircraft could accelerate vertically and to account for any voltage sag. The propellers were required to be less than 56 cm (22 in) to ensure that the propellers would fit within the competition size requirements without

interfering with the structure of the aircraft. The results for the maximum thrust of each of the configurations tested are shown in Table 5.

ESC	Motor	Propeller			
Max Thrust (g) > 5150 g		20x6	MF2211	V22x7.4	21.5x7.3x3
KDE 55A	MN501-S KV300	3800	4900	4880	5060
	MN505-S KV320	5080	6560	6500	6400
	KDE5215 KV220	2960	N/A	4300	4570
T-Motor Flame 70A	MN501-S KV300	4040	5450	5290	5270
	MN505-S KV320	5040	6610	6750	6360
	KDE5215 KV220	2960	N/A	4110	4250

Table 5. Test matrix showing maximum thrust of propulsion system configurations. Green cells represent configurations that met the 2:1 TWR requirement, red cells represent configuration that did not

The 2:1 TWR was only met by the MN501-S and the MN505-S motors. To reduce weight, the MN501-S was selected over the MN505-S, as the MN501-S is 55g less than the MN505-S. When selecting the propeller, only the V22x7.4 and MF2211 supplied enough thrust when paired with the MN501-S. While the MF2211 supplied more thrust than the V22x7.4, both met the 2:1 TWR and had similar power and current performances. The V22x7.4 was 23g lighter and had a lower power draw than the MF2211; therefore, the V22x7.4 propeller was selected. The Flame 70A ESC was selected as it offered increased performance over the KDE55A and was 10g lighter. Thus, the final propulsion configuration consists of the MN501-S motor, the V22x7.4 propeller, and the Flame 70A ESC.

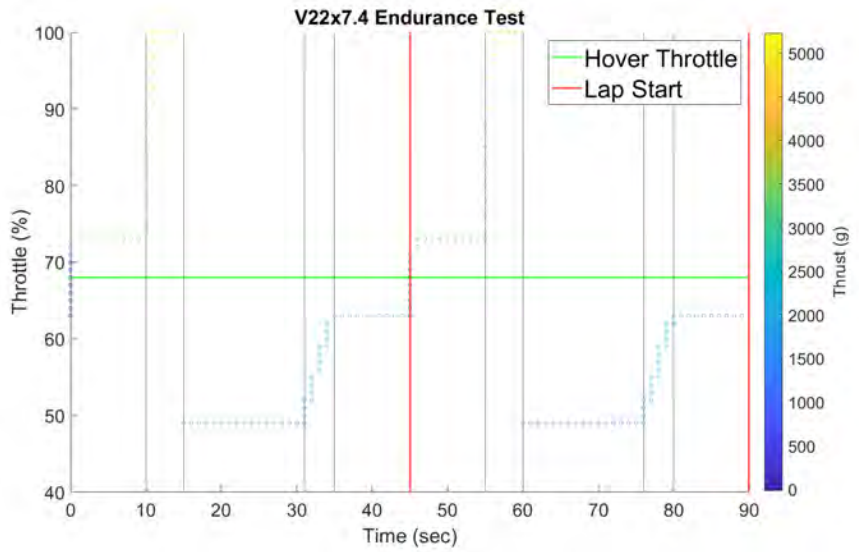

Figure 11. Outline of the endurance mission profile

To verify that the propulsion system can withstand the full length of the endurance mission without overheating, the team ran a bench test to simulate the mission profile of the flight. This test represents a worst case scenario for the as the cruise power was overestimated and there was no additional airflow over the motor to help cool the motor. Two laps of the mission profile are shown in Figure 11. The team estimated 10 seconds for takeoff at 5% throttle above hover throttle, leading to a vertical acceleration of 2 m/s^2. Next, there is a 5 second transition at full throttle to accelerate to cruise speed before dropping to a constant 150 W of power draw to imitate cruise flight. After holding cruise power for 16 seconds to

simulate flying a lap, the throttle increased to 5% below hover to simulate deceleration and landing of the aircraft. This was repeated for the duration of 10 minutes and monitored the temperature of the motor casing using an infrared thermal camera.

The test was run in 10℃ ambient conditions and found that the motor reached a maximum temperature of 60℃ at the end of the test. The motor is rated for 180℃ in the stator coils and 220℃ for the permanent magnets in the casing. With this test, it was determined that the motor has a significant safety factor before failure, even with the assumption that the stator is 20℃ above the casing. After running this test three additional times with a cooling period between each test, the maximum temperature was very consistent between each test, so the team is confident that the propulsion system will be able to withstand the endurance test without overheating.

4.3 Power System

To verify the power system, multiple brands of batteries were tested in throttle holds at varying levels and a simulation of the mission profile for the endurance course. Based on initial power draw prediction, the aircraft would be able to complete a 12 minute flight by fully draining the 3 4000-mAh batteries onboard. During testing, however, the motor and propeller combination proved to be more efficient, allowing for a 16 minute run of the simulated endurance course. Thus, MVFT found that it can reduce the size of the propulsion batteries to 3 3300-mAh LiPos in parallel. This will provide the craft with 13.5 minutes of flight in the endurance course, well beyond the 10 minutes allowed and retaining a safe amount of reserve power to land.

The batteries tested included the Onyx 6s 4000mah 30C LiPo and the Admiral 6s 4000mah 40C LiPo. There was no measurable difference between the Onyx and Admiral LiPo batteries performances. Each outputted the necessary current to power the aircraft and lasted for approximately 16 minutes of flight time. With both batteries showing nearly identical performance it came down to the physical attributes differentiating the packs. The Admiral battery came in 20g lighter and 12000mm^3 smaller so it was selected for the aircraft. Testing showed a decreased need in battery capacity so 3 3300-mAh 6s LiPos were purchased. These batteries will save an additional 150g, allowing for more payload.

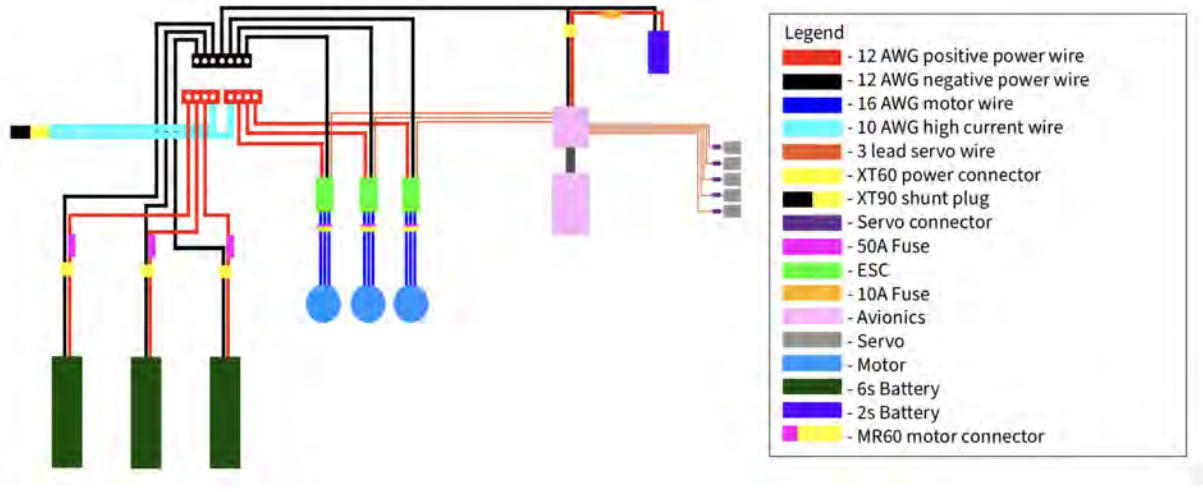

Figure 12. Competition Aircraft Electrical Schematic

The rest of the system includes the bus bars, power wiring and the shunt plug, shown in Figure 12. Due to the relatively high current draw of the system, 12AWG wire was selected for all the power wiring from

each battery to the bus bars and from the bus bars to the ESCs. Because all the current running through the system must pass through the shunt plug, 10AWG wire was used to handle the large current flow. Each propulsion battery is fused with a 32V 50A blade style fuse, below the 120A max discharge rating of the batteries. Similarly the avionics battery has a 10A fuse and a max discharge rating of 12A.

4.4 Avionics

The major components of the avionics package have not changed from MVFT's previous VFS PDR submission. All five servos (three tilt mechanisms and two elevons) and ESCs are connected to the power distribution board's PWM outputs. The Pixhawk 4 used by MVFT makes use of the ArduPilot software and the aircraft runs under an ArduPlane configuration, using parameters to define the aircraft's behavior and configuration. For example, the lost-link power cut feature is programmed through the AFS_ENABLE parameter, enabling the use of AFS_TERM_ACTION parameter which immediately terminates the flight and crashes the plane when GPS, telemetry or RC control is lost (AFS_WP_GPS_LOSS, AFS_WP_COMMS, and AFS_RC_FAIL_TIME, respectively).

The navigator uses GPS to assist the pilot during every flight using the MissionPlanner software (Figure 13). This software is used to program parameters to the Pixhawk which define the aircraft's behavior, such as the maximum angle servos tilt to maximize yaw authority while avoiding propeller strikes. MissionPlanner is also used to plan autonomous flights, using GPS waypoints and commands to the vehicle such as Takeoff, Waypoint, Spline Waypoint, and Land. These waypoints allow for complex autonomous navigation, proven using the quadcopter platform in the March 7th flight test (Figure 13), in which the quadcopter flew a spline figure-8 autonomously, while changing altitudes at each waypoint.

The transition from vertical to cruise flight is handled automatically by the Pixhawk once the pilot, through a transmitter switch or the navigator, through MissionPlanner, sends the command to the aircraft to switch modes from Q_STABILIZE (stabilized flight in hover) to FBWA (fly-by-wire with manual throttle control). The transition process initiates when the aircraft increases the throttle to gain speed horizontally, while simultaneously slowly tilting the motors to 45 degrees, entering its transition stage. Once the transition speed is reached as measured by the pitot tube, the motors will tilt another 45 degrees to attain the desired horizontal configuration. When transitioning from cruise to vertical flight, the motors will immediately stop and return to their vertical position while the plane slows down, stability is maintained by the control surfaces, and attitude control is also provided as needed.

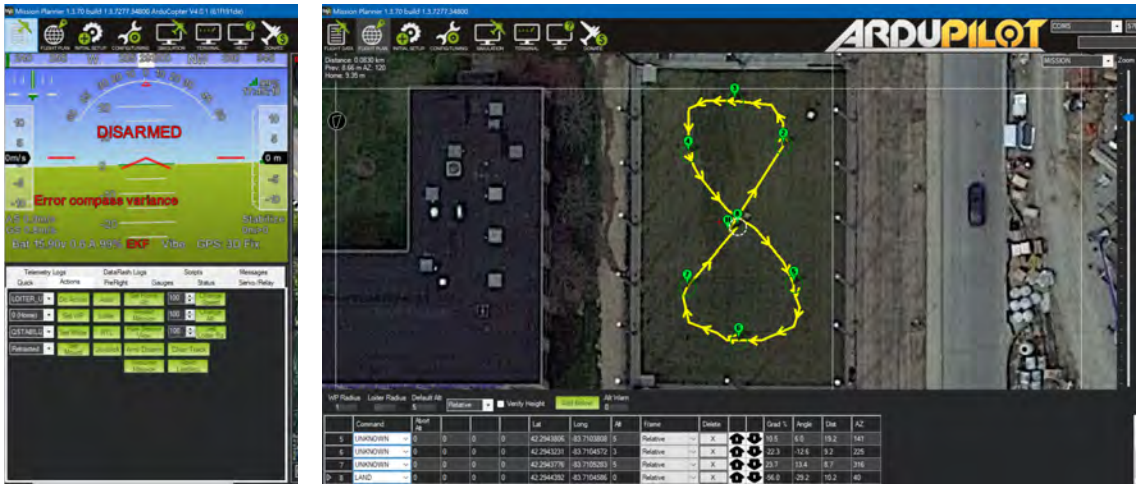

Figure 13. MissionPlanner Navigator Example (top) & Quadcopter Autonomous Flight Path (bottom)

5. Drawing Package

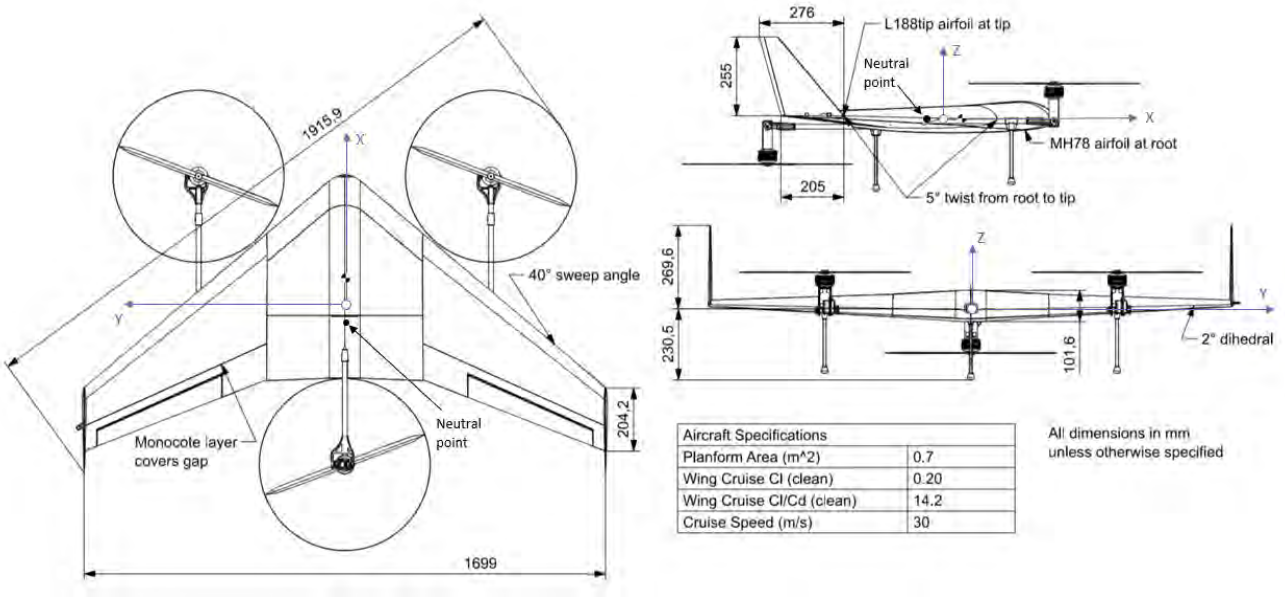

Figure 14. 3-view of aircraft and aerodynamic specifications

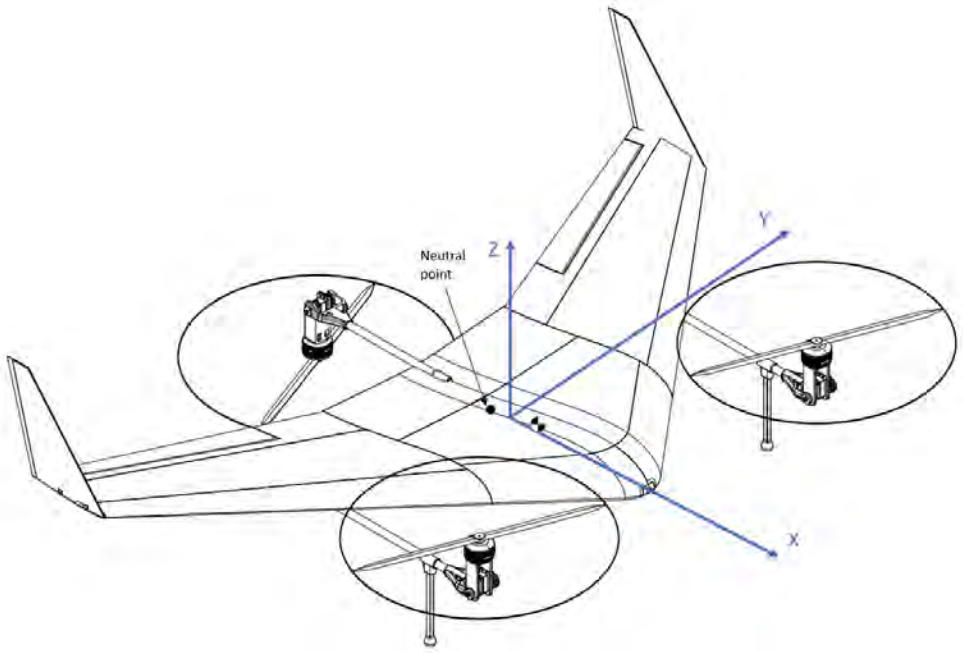

Figure 15. Aircraft isometric view

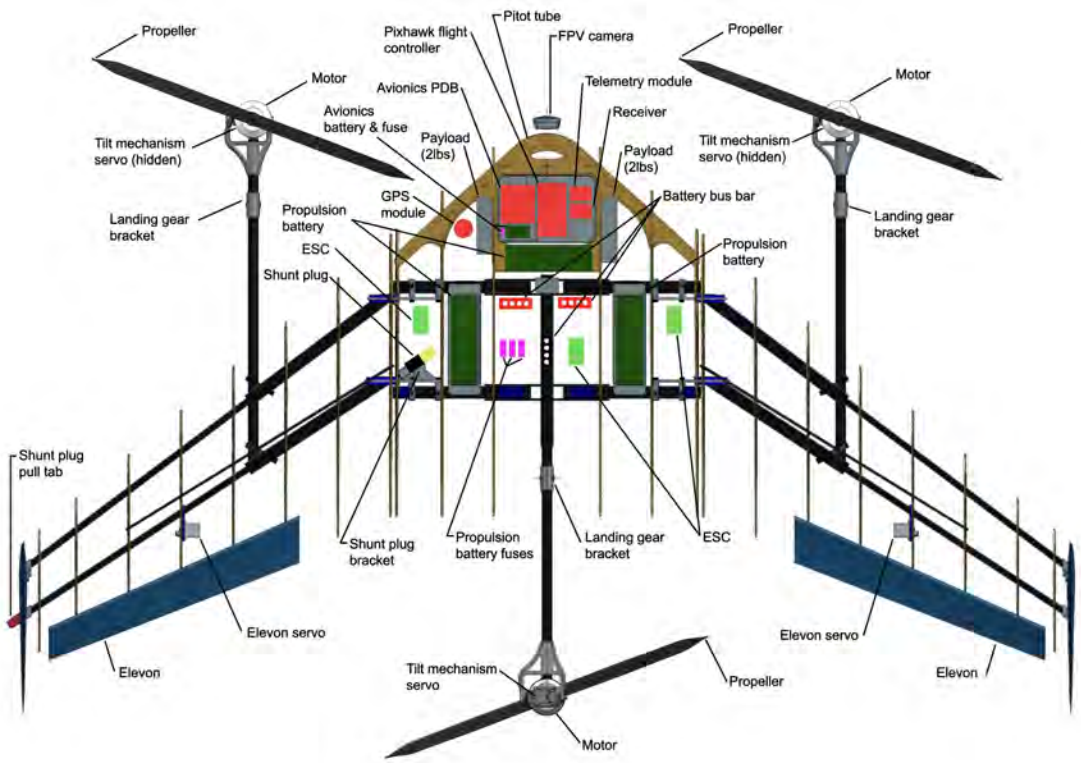

Figure 16. Structural, power, and avionics layout with callouts

6. Fabrication Methods

All parts of the main airframe were designed and fabricated in-house using composites. The primary facility that MVFT utilizes for manufacturing is the Wilson Student Team Project Center (Wilson Center), in addition to the Second-Year Aero Lab and Systems Engineering Leadership Lab. These facilities provide all of the manufacturing and assembly resources that the team required which include mill operations, CNC machining, 3D-printing, and vacuum pumps for composite layups. For each specific operation, MVFT has trained members to complete the manufacturing of custom parts. Based on previous prototyping, the team has focused on design for manufacturing in each component's shape and material. Table 5 details the material, stock, and fabrication methods of each part of the airframe.

Part name	Material	Stock	Fabrication	Tools
Spars	Pultruded Carbon Fiber	Cured square stock	Cut to length	Abrasive cutter
Gussets	Twill 3k Carbon Fiber	Cured 6-mm plate	Cut following pattern	Abrasive cutter
Ribs	Basswood	3-mm sheet	Laser cut	Laser cutter
Shell	Kevlar 49 Twill Weave, West System 105 Epoxy Resin/205 Fast Hardener	Kevlar fabric, epoxy resin kit	Apply PVA on mold, cut adequate shape, layup (epoxy), trim	Kevlar scissors, mold, vacuum bag and pump
Leading/trailing edges	Balsa wood	0.8-mm sheet	Bend around ribs	Utility knives
Wing attachment block - interior	6061 Aluminum	25x50x50-mm block	Milled, threaded	Mill, tap
Wing attachment block - exterior	6061 Aluminum	5-mm sheet	Milled	Mill

Table 6. Part materials and descriptions of purchased stock, fabrication methods, and required tools for fabrication of the airframe.

MVFT worked with the Taubman Fabrication Lab, a local University of Michigan facility, to form the molds for composite layups. One of these molds is shown in Figure 17. For construction of composite parts, MVFT performed vacuum-bagged wet layups. This process involved preparing the molds with parting wax and PVA release film, wetting the kevlar with the epoxy resin and removing the excess, laying the kevlar into the molds, adding layers of nylon release peel ply and polyester bleeder fabric, respectively, closing the mold in a vacuum bag, and applying the vacuum to sit for 24 hours.

Special attention was taken with the assembly of the aircraft's inner frame. This structure had very few right angles or convenient reference points to measure against during assembly, making it difficult to ensure that the prescribed orientations of parts are achieved. To make it possible to properly assemble this structure, a jig was constructed to hold the parts in their prescribed orientations while the epoxy set. This jig, shown with the frame installed in Figure 17, consisted of a single flat wooden base plate with pedestals designed to hold the frame parts at the necessary orientations.

With this jig, key areas of the frame could be assembled and bonded at one time to ensure that proper alignment was achieved and tolerance stackups were avoided. Once the inner frame was assembled, the body shell, leading and trailing edges, and monokote could then be applied. The body shell and edges were applied first by using epoxy to permanently attach them to the ribs. A layer of monokote was then stretched over the gaps on the wings, creating a light yet effective aerodynamic surface. After this step, the airframe was complete. The completed airframe is shown in Figure 18.

Figure 17. Layup molds machined from medium-density foam (left) and the frame bonding jig with frame installed (right)

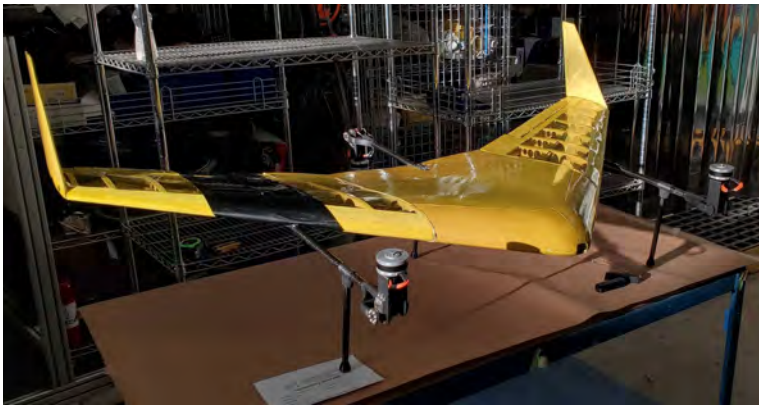

Figure 18. Completed airframe

7. Test Plan

7.1 Tilt Corridor Wind Tunnel Testing

To improve the transition from vertical to horizontal flight, the team plans to perform wind tunnel tests with the 4-lb prototype in order to determine the tilt corridor for the motor configuration, defining limits of tilt angle and acceleration as a function of airspeed [12]. These tests will consist of running the wind tunnel at various speeds and tilt mechanism angles (0 to 90 from horizontal in increments of 10), measuring the resulting forces in 3 axes for a chosen throttle. These tests will enable the team to determine the optimal angle, tilt rate and throttle for the transition stage mentioned in section 4.4.

7.2 Custom Thrust Stand and Sensor Package

The motor, propeller, and ESC configurations were tested using a custom thrust testing stand and sensor package. The stand is an L-shaped design, shown in Figure 19, with the motor mounted on the vertical arm to keep it away from any flow obstructions. The thrust of the propeller was measured using a load cell mounted below the horizontal arm with a pivot at the base of the L to transfer the force. The torque is measured via a second load cell connected to the motor mount placed on a pivot coaxially with the motor shaft. The motor mount is then restrained by the load cell a known distance away so the torque could be calculated from the force measurement.

The team also developed a custom sensor package capable of measuring thrust, torque, voltage and current. The sensor package can send throttle signals to the ESC to control the motor the same way for every test. The sensor package can be controlled and monitored wirelessly from a computer, so the tests can be performed from a safe distance away. During testing, the team can select different testing profiles to automatically run the motor through all throttle values, a constant throttle for a given amount of time, or a simulation of the 10-minute endurance flight mission profile. The data from each of these tests is fed back to the computer in a comma-separated table that can be recorded and analyzed later in MATLAB.

Before each day of testing standard procedures were completed to ensure accurate and useful data. The thrust load cell was calibrated by attaching a weight to the motor mount and letting it hang over a pulley to pull on the vertical arm. Since the load cell follows a linear calibration curve, the slope of the curve can be fine tuned until the output matches the calibration weight. The torque load cell was calibrated similarly by mounting a known weight on a moment arm away from the pivot to apply a calibrated torque value. Both the thrust and torque load cells were zeroed before the start of each test to account for any offset from the weight of the motor. The voltage sensor was calibrated each day by measuring the battery voltage prior to connecting it to the sensor package and comparing the output data.

Finally, the current sensor was zeroed by measuring the signal from the sensor before the battery was connected and the calibration curve was based on the specifications from the sensor manufacturer. Daily calibrations help build confidence that the data received from the tests are representative of the actual performance of the system. This was further verified by the test with the KDE5215 Motor, KDE 55A ESC, and 21.5x7.3x3 propeller since the manufacturer provides data for this exact configuration on a 6s battery and the team found that the maximum thrust was within 2% of the manufacturer test.

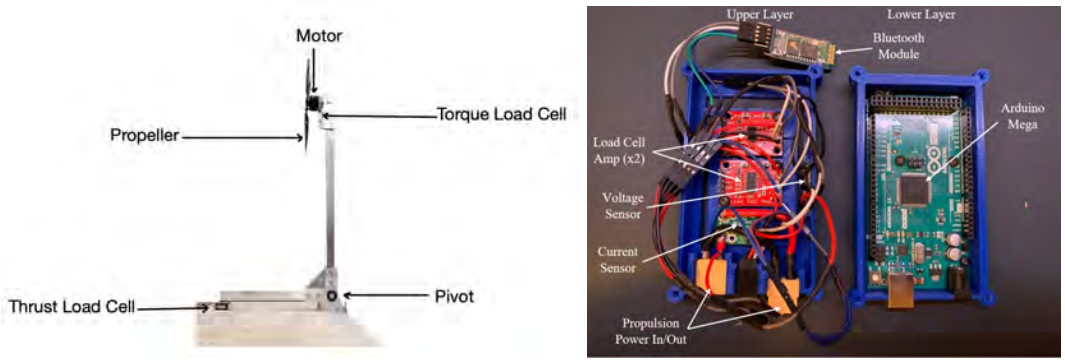

Figure 19. Overview of the thrust stand and sensor package

7.3 Flight Tests

7.3.1 NM-1 Prototype

The NM-1 prototype has been used to verify the controllability and maneuverability of the motor configuration in hover. The team has plans to verify the transition procedure with the university pilot at Flying Pilgrims RC club, as well as perform cruise flight maneuvers (banked turns, ascensions and descents) to validate the elevon control surfaces on a delta wing. The goal of these tests will be to determine the transition profile, minimum airspeed needed to cruise speed as well as controllability when transitioning to and from cruise flight. In addition, there are plans to utilize the M-Air testing facility to perform autonomy maneuver flights as well as landing accuracy tests like the quadcopter flights.

7.3.2 Competition Aircraft

The testing plans for the competition aircraft will follow the flight tests performed by the prototype. First, hover tests will be performed at M-Air to verify the control authority in roll, pitch and yaw. These flights will aim to gauge the pilot's ability to control the aircraft in flight as well as accurately land. Once hover stability and control has been established, transition flights will be performed by the university's professional pilot at Flying Pilgrims RC club. These flights, like the prototype's, will aim to confirm the transition profile and estimated transition speed from the wind tunnel tests as well as control surface control authority and differential thrust assistance for yaw control. Lastly, autonomous flight tests similar to the competition's autonomous challenge will be conducted, applying the proposed improvements to autonomous landing accuracy from the quadcopter tests.

8. Flight Test Results

MVFT currently has two aircraft in addition to the proposed solution. The autonomy quadcopter shown below is a low-risk autonomy test platform to verify GPS-guided navigation in autonomous flight. The prototype (middle) is used to verify the motor configuration and controls for the proposed solution.

Figure 20. The flight test vehicle fleet (left to right) includes the autonomy quadcopter, sub-scale prototype, and competition aircraft

8.1 NM-1 Prototype

The flights performed with the prototype verify the roll, pitch, and yaw control and stability in hover using the direct-drive servo-controlled tilt mechanisms. MVFT increased yaw authority by increasing the angle tilted back from approximately 15 to 20 degrees. Additionally, the team improved the test flight report templates to include important information needed to assess the success of test flights, as well as implementing a spreadsheet to track the completion of test flights for each vehicle in the fleet.

Previously, the plan was to use a rack and pinion mechanism so that the servo did not take up space underneath the propeller. This was less efficient than the direct-drive, for the gears were less sensitives and slipped on the rack. In addition, the maintenance required by the rack and pinion mechanism is not feasible for the larger scale aircraft. Thus, the direct-drive solution was chosen for the final aircraft.

8.2 Autonomous Quadcopter Tests

MVFT conducted autonomous flights with the quadcopter to verify the accuracy of landing after performing a mission. This test was performed by performing a diamond-shaped flight in the cardinal directions of M-Air and landing at the takeoff point, marked by tape. Once the aircraft landed, the distance from goal and final positions was recorded.

Figure 21 displays the 60% accuracy over 10 autonomous landings with the competition landing pad size for reference. Improvements to accuracy include: weather vaning to avoid wind drifting, decreasing the waypoint radius (1-m shown in plot), and manually inputting GPS coordinates rather than using the user interface.

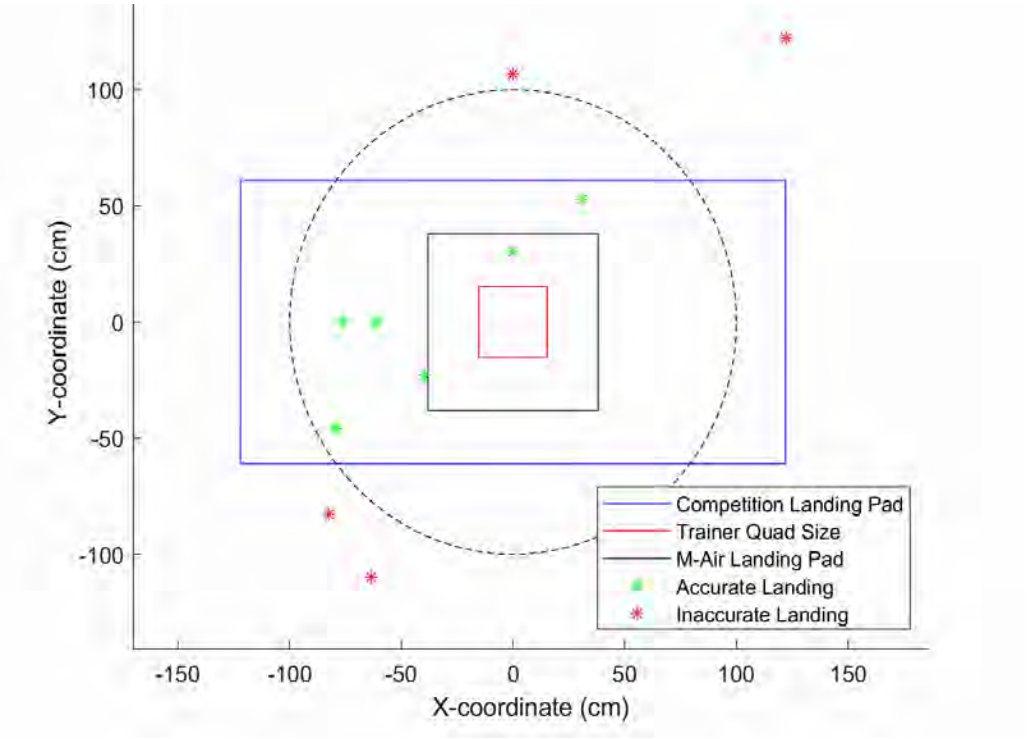

Figure 21. Quadcopter Autonomous Landing Accuracy Test Results

Works Cited

[1] APC Propellers. 2020. *Performance Data | APC Propellers*. [online] Available at: <https://www.apcprop.com/technical-information/performance-data/> [Accessed 17 December 2020].

[2] "Chapter 11: Aircraft Performance," in Pilot's handbook of aeronautical knowledge, Washington, D.C.: U.S. Department of Transportation, Federal Aviation Administration, Flight Standards Service, 2020.

[3] "Connect ESCs and Motors¶," ArduPilot Copter documentation, 2020. [Online]. Available: https://ardupilot.org/copter/docs/connect-escs-and-motors.html. [Accessed: 20-Dec-2020].

[4] 11.7 Performance of Propellers. [Online]. Available: https://web.mit.edu/16.unified/www/FALL/thermodynamics/notes/node86.html. [Accessed: 20-Dec-2020].

[5] S. Addarkaoui, A. Bernier, Y. Chen, H. Compere, A. Dore, M. Fransolet, R. Jumpertz, and L. Macchiaiolo, "Graduate Team Aircraft Design Competition: Electric Vertical Takeoff and Landing (E-VTOL) Aircraft Mistral Air Taxi," *AIAA GRADUATE TEAM AIRCRAFT DESIGN COMPETITION 2018-2019*. <https://www.aiaa.org/docs/default-source/uploadedfiles/education-and-careers/university-students/design-competitions/3rd-place-grad-team-aircraft.pdf?sfvrsn=5d49f2cf_0>

[6] J. L. Palmer, "Assembly and Initial Analysis of a Database of the Characteristics of Fixed-Wing Unmanned Aircraft Systems." Victoria, 2015. <https://apps.dtic.mil/dtic/tr/fulltext/u2/a623605.pdf>

[7] Bhphotovideo.com. 2020. *YUNEEC Tornado H920 Hexa-Copter With ST24 Transmitter*. [online] Available at: <https://www.bhphotovideo.com/c/product/1190628-REG/yuneec_yunh920us_tornado_h920_hexa_copter_with.html/specs?SID=kit4qufqq30002cl02fa9> [Accessed 17 December 2020].

[8] Allen, B., 2020. *Blended Wing Body Fact Sheet*. [online] NASA. Available at: <https://www.nasa.gov/centers/langley/news/factsheets/FS-2003-11-81-LaRC.html> [Accessed 17 December 2020].

[9] D. P. Raymer, "Weights," in *Aircraft Design: a Conceptual Approach*, Washington, D.C.: American Institute of Aeronautics and Astronautics, 1992, pp. 404–405.

[10] M. Drela and H. Youngren, *AVL*. MIT.

[11] D. P. Raymer, "Initial Sizing," in *Aircraft Design: a Conceptual Approach*, Washington, D.C.: American Institute of Aeronautics and Astronautics, 1992, pp. 113.

[12] Z. Liu, Y. He, L. Yang, and J. Han, "Control techniques of tilt rotor unmanned aerial vehicle systems: A review," *Chinese Journal of Aeronautics*, vol. 30, no. 1, pp. 135–148, Feb. 2017.